2015 American Control Conference
Palmer House Hilton
July 1-3, 2015. Chicago, IL, USA

Combined Vector Field Approach for Planar Curved Path Following with Fixed-Wing UAVs

Yueqian Liang, Yingmin Jia, Zhuo Wang and Fumitoshi Matsuno

Abstract— **In this paper the problem of planar curved path following using fixed-wing unmanned aerial vehicles (UAVs) is studied. UAV input constraints and constant wind disturbance are considered. A combined vector field is proposed by trading off a conservative vector field and a solenoidal vector field. Accordingly a saturated course rate controller is designed, and its stability is discussed through the Lyapunov stability theory. Simulation examples show us the effectiveness of the approach.**

I. INTRODUCTION

Unmanned aerial vehicles (UAVs) have now been successfully applied in both military and civilian areas, such as search and rescue, fire detection, traffic monitoring, filmmaking, reconnaissance, surveillance, convoy protection, target tracking and so on [1]. The largest difference between a UAV and a manned aerial vehicle is that a UAV must rely on its own autonomy capability to accomplish varieties of missions, which often requires the UAV to generate mission paths and then to accurately follow them [2], [3], [4]. The latter aspect requires good path following capability of the UAVs.

During the past few years, to address the path following problem, guidance vector field approach has been paid much attention due to its great convenience. That is, it provides desired flight path angles and further feasible reference paths for the UAV to track. As a particular case, the circular path following, also referring to as standoff target tracking [5], in which the UAV is steered to maintain a certain loitering circle with respect to a certain center (usually the target position), is widely considered. Vector field method was first proposed by Lawrence and Frew *et al.* to achieve the standoff tracking [5], [6]. By tracking the globally convergent Lyapunov guidance vector field, heading rate is commanded to follow the circular path moving with the target [5]. And by further considering the heading error with respect to the vector field, a more accurate feedforward term is exploited to obtain more accurate circular path following in [7], [8]. Recently Zhu *et al.* gave the rigorous proof of the global convergence of the vector field based circular path following [9]. By combining Lyapunov guidance vector field with a tangent vector field, Chen *et al.* further considered this problem temporally to get a theoretically shortest path [10]. Other innovative aspects for the circular path following can be found in some recent works [11], [12], [13], [14].

This work was supported by the National Basic Research Program of China (973 Program: 2012CB821200, 2012CB821201) and the NSFC (61134005, 61221061, 61327807, 61304232).

Y. Liang and Y. Jia are with the Seventh Research Division and the Center for Information and Control, Beihang University (BUAA), Beijing 100191, China (e-mails: liangyueqian3002@126.com; ymjia@buaa.edu.cn).

Z. Wang is with the Department of Chemical and Biomolecular Engineering, Hong Kong University of Science and Technology, Clear Water Bay, Kowloon, Hong Kong (e-mail: zhuowang@ust.hk).

F. Matsuno is with the Department of Mechanical Engineering and Science, Kyoto University, Kyoto 606-8501, Japan (e-mail: matsuno@me.kyoto-u.ac.jp).

The circular path is one kind of curved paths, the path following of which was studied by Nelson and Griffiths *et al.* in Refs. [2], [15], where they put forward the tangent vector fields. Based on them, sliding mode controllers were designed for the course to achieve the curved path following given constant wind disturbances. However the slide mode controller is known to suffer the chattering problem due to the controller's inherent discontinuity [16]. Moreover the input constraints of UAVs [17], [18], e.g., saturated course rate, should be explicitly considered.

Motivated by the above discussions, by explicitly taking UAV input constraints into account, this paper aims to design a saturated controller for the planar curved path following problem based on a newly proposed combined vector field. The remainder of this paper is organized as follows. Section II formulates the planar curved path following problem. The combined vector field approach is elaborated in Section III, along with the detailed discussion of the controller stability. In Section IV simulation examples are presented to assess the proposed approach. Finally we give a short conclusion in the last section.

II. PROBLEM FORMULATION

Fixed-wing UAVs equipped with low-level flight controllers, which can provide course- and altitude-hold functions, are assumed to be used for the path following mission. The altitude is held constant through zero climb rate. The airspeed is assumed to be constant from the fuel efficiency and mission duration points of view. Steady background wind disturbance is assumed to be present during the path following mission.

The kinematics of the UAV in inertial XY frame in the presence of wind can be modeled as the following Dubins equations

$$\dot{x} = V_a \cos\psi + W_x \tag{1}$$

$$\dot{y} = V_a \sin\psi + W_y \tag{2}$$

$$\dot{\psi} = u_0 \tag{3}$$

where $\mathbf{p} = (x, y)^T$ is the inertial position of the UAV, $\mathbf{v} = (\dot{x}, \dot{y})^T$ denotes the inertial horizontal velocity, $\psi \in (-\pi, \pi]$ is the UAV heading, V_a is the constant airspeed, and $\mathbf{W} = (W_x, W_y)^T$ is the wind velocity. As usual the wind speed W

is assumed to be less than the airspeed V_a. u_0 represents the commanded heading rate, satisfying the constraint

$$|u_0| \le \dot{\psi}_{\max} \tag{4}$$

Note that the magnitude of $\mathbf{v}$ is the groundspeed, which is denoted as V_g.

Introducing the course χ, (1)-(3) can be equivalently expressed as

$$\dot{x} = V_g \cos\chi \tag{5}$$

$$\dot{y} = V_g \sin\chi \tag{6}$$

$$\dot{\chi} = u_1 \tag{7}$$

where u_1 is the course rate input. The relation between heading rate and course rate is given by

$$u_1 = L(\psi)u_0 \tag{8}$$

where

$$L(\psi) = \frac{V_a^2 + V_a\left(W_x\cos\psi + W_y\sin\psi\right)}{V_a^2 + W_x^2 + W_y^2 + 2V_a\left(W_x\cos\psi + W_y\sin\psi\right)} \tag{9}$$

It can be easily seen that $L(\psi) \in (1/2, 1)$. From (8) we can see that there also exists a constraint on the course rate, which is assumed to be

$$|u_1| \le \dot{\chi}_{\max} \tag{10}$$

As an example, $\dot{\chi}_{\max}$ can be set as $\dot{\psi}_{\max}/2$.

Denote the path to be followed as C_2, and it is assumed to be an arbitrary smooth curve or a piecewise smooth curve. It can be modeled as $f(x, y) = 0$. To measure the closeness of the current UAV position $\mathbf{p}$ to the desired path, we define a directional distance between them as $r = f(\mathbf{p}) = f(x, y)$. Large $|r|$ implies large distance between them, and $r = 0$ means that $\mathbf{p}$ locates right on the desired path.

The planar curved path following problem can now be summarized as: To design input commands u_1 for the fixed-wing UAV whose kinematics model is given in (5)-(7) such that 1) the input constraints (10) holds, and 2) if possible, make the UAV fly along the desired path, and if not, make the distance r as small as we can.

III. COMBINED VECTOR FIELD APPROACH

A. Conservative Vector Field and Solenoidal Vector Field

It is known from the Helmholtz theorem that an arbitrary vector field can be decomposed into two parts, i.e., conservative part and solenoidal part. Conservative part is irrotational which can usually be given as the gradient of a scalar function, while solenoidal part is a rotational one which can be expressed as the curl of a vector function.

Consider a scalar potential $f_c = \sqrt{f^2(x, y) + 1}$. Its gradient determines a conservative vector field. Normalizing this gradient, we can get a conservative vector field as

$$\mathbf{v}_c = \frac{1}{\sqrt{f_x^2 + f_y^2}}\begin{pmatrix} f_x \\ f_y \end{pmatrix} \tag{11}$$

where f_x and f_y are partial derivatives of f with respect to x and y respectively. We can see that (11) is actually independent of the potential f_c.

Tangential vector field of curve C_2 can be chosen as its solenoidal vector field. Specifically, a normalized solenoidal vector field for C_2 is given by

$$\mathbf{v}_s = \frac{1}{\sqrt{f_x^2 + f_y^2}}\begin{pmatrix} f_y \\ -f_x \end{pmatrix} \tag{12}$$

It can be seen that the two vector fields (11) and (12) are perpendicular to each other at each point of the 2D space, since we have $\mathbf{v}_c \cdot \mathbf{v}_s = 0$. Actually $\mathbf{v}_s$ aligns with the tangential direction of a point on the curve C_2, while $\mathbf{v}_c$ is the normal direction at the same point.

B. Vector Field Combination

When we have the conservative vector field (11) and the solenoidal vector field (12), according to Helmholtz decomposition, if we can generate a combined vector field such that for each point $\mathbf{p}$ in this field, when it locates very far away from the desired curve C_2, its vector aligns with the conservative vector field (11) to travel directly to the desired path, and when $\mathbf{p}$ is on the curve C_2, its vector aligns with the solenoidal vector field (12), i.e., along the desired path, then the curved path following can be achieved.

We combine these two vector fields as the following form

$$\begin{aligned}\mathbf{v}_d = (\dot{x}_d, \dot{y}_d)^T &= -\tanh(\kappa r)\,\mathbf{v}_c + s\,\mathrm{sech}(\kappa r)\,\mathbf{v}_s \\ &= \frac{1}{\sqrt{f_x^2 + f_y^2}}\begin{pmatrix} -f_x\tanh(\kappa f(x, y)) + s f_y \mathrm{sech}(\kappa f(x, y)) \\ -f_y\tanh(\kappa f(x, y)) - s f_x \mathrm{sech}(\kappa f(x, y)) \end{pmatrix}\end{aligned} \tag{13}$$

where κ is a positive scaling factor, and $s = \pm$ determines the direction of the vector field. For example, if C_2 is a circle, then choosing "+" gives a clockwise vector field, while choosing "−" generates a counter-clockwise vector field. Noticing that $\tanh^2(x) + \mathrm{sech}^2(x) = 1$, it can be easily seen that this vector field is normalized. Furthermore it can be verified that the above requirements are satisfied. Examples of the above vector fields are illustrated in Fig. 1.

We state that any desired path determined by vector field (13) initiating from an arbitrary location in the space asymptotically converges to the corresponding curve C_2. In fact, consider a Lyapunov function candidate $V_1 = r^2/2$, and evaluating its time derivative along this vector field yields

$$\dot{V}_1 = r\dot{r} = -f\tanh(\kappa f)\sqrt{f_x^2 + f_y^2} \tag{14}$$

It can be easily seen that $\dot{V}_1 \le 0$ satisfies for all f. Then the Lyapunov's direct method can be invoked to give us that $r \to 0$, which implies the satisfaction of the above statement.

C. Controller Design

The desired course determined by the combined vector field (13) can be computed as

$$\chi_d = \mathrm{arctan2}(\dot{y}_d, \dot{x}_d) \tag{15}$$

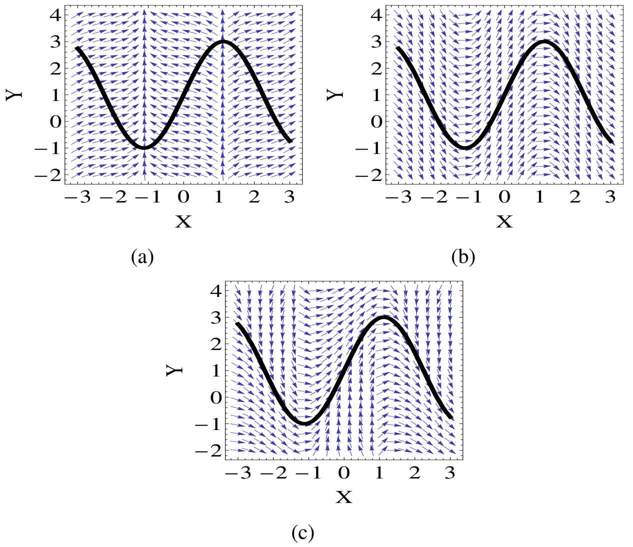

Fig. 1. Vector fields for the sine curve $y = 2\sin(1.4x) - 1$: (a) Conservative vector field; (b) Solenoidal vector field; (c) Combined vector field.

Its time derivative is given by

$$\dot{\chi}_d = V_g \mathcal{A}_1 \cos\chi + V_g \mathcal{A}_2 \sin\chi \tag{16}$$

where

$$\mathcal{A}_1 = -\kappa f_x \operatorname{sech}(\kappa f) - (f_{xx} f_y - f_x f_{xy}) \Big/ \sqrt{f_x^2 + f_y^2} \tag{17}$$

$$\mathcal{A}_2 = -\kappa f_y \operatorname{sech}(\kappa f) + (f_{yy} f_x - f_y f_{xy}) \Big/ \sqrt{f_x^2 + f_y^2} \tag{18}$$

Denote the course error between the UAV and the combined vector field (13) as $\chi_e = < \chi - \chi_d > \in (-\pi, \pi]$. Note that this error has been considered by (16). Considering the input constraint, we design a saturated course rate controller for the path following problem of the curve path C_2 as

$$u_1 = \dot{\chi}_{max} \operatorname{sat}\left(\frac{-k_\chi \chi_e + \dot{\chi}_d}{\dot{\chi}_{max}} \right) \tag{19}$$

where k_χ is a positive feedback gain, and

$$\operatorname{sat}(x) = \begin{cases} x, & \text{if } |x| \le 1 \\ \operatorname{sgn}(x), & \text{otherwise} \end{cases} \tag{20}$$

is the saturation function.

D. Stability Analysis

The main result of the controller stability is given in the following theorem.

Theorem 1: Considering the UAV kinematics system (5)-(7) and the saturated course rate controller given in (19), under the condition

$$|\mathcal{A}_1| + |\mathcal{A}_2| \le \frac{7\dot{\chi}_{\max}}{10 V_g} \tag{21}$$

the UAV trajectory asymptotically converges to the curve C_2. That is, as the time $t \to \infty$, both the directional distance r and the course error between UAV and the desired curve converge to zero.

Before giving its proof, we present three useful lemmas as below. It needs to be noted that all the proofs given below are based on the sign choice $s = +$ for (13), and the proofs corresponding to the other sign choice are very similar.

Lemma 1: Given (21), there exists a positive constant k_1 for the desired course rate (16) such that

$$\begin{cases} \dot{\chi}_d \ge -\dot{\chi}_{\max} + k_1 \sin\chi_e, & \text{if } \chi_e \in (0, \pi] \\ \dot{\chi}_d \le \dot{\chi}_{\max} + k_1 \sin\chi_e, & \text{if } \chi_e \in (-\pi, 0] \end{cases} \tag{22}$$

Proof: The conclusion can be drawn from three cases.

CASE 1. $\chi_e \in (0, \pi)$

In this case, we have $\sin\chi_e \in (0, 1)$. Consider the function

$$\begin{aligned} F(\chi_e) &= \frac{1}{\sin\chi_e} (\dot{\chi}_d + \dot{\chi}_{\max}) \\ &= V_g (\mathcal{A}_1 \cos\chi_d + \mathcal{A}_2 \sin\chi_d) \cot\chi_e + \dot{\chi}_{\max} \csc\chi_e \\ &\quad + V_g (-\mathcal{A}_1 \sin\chi_d + \mathcal{A}_2 \cos\chi_d) \end{aligned} \tag{23}$$

Differentiating this function with respect to χ_e yields

$$\frac{\mathrm{d}F(\chi_e)}{\mathrm{d}\chi_e} = \frac{-V_g (\mathcal{A}_1 \cos\chi_d + \mathcal{A}_2 \sin\chi_d) - \dot{\chi}_{\max} \cos\chi_e}{\sin^2\chi_e} \tag{24}$$

Letting the derivative be zero, we have

$$\cos\chi_{e0} = -\frac{V_g (\mathcal{A}_1 \cos\chi_d + \mathcal{A}_2 \sin\chi_d)}{\dot{\chi}_{\max}} \tag{25}$$

From (21) and (25), we have

$$|\cos\chi_{e0}| \le \frac{V_g (|\mathcal{A}_1| + |\mathcal{A}_2|)}{\dot{\chi}_{\max}} \le \frac{7}{10} \tag{26}$$

$$\sin\chi_{e0} = \sqrt{1 - \cos^2\chi_{e0}} \ge \sqrt{51}/10 \tag{27}$$

Computing the second derivative of $F(\chi_e)$ and substituting (25) and (27) into it, we obtain

$$\frac{\mathrm{d}^2 F(\chi_e)}{\mathrm{d}\chi_e^2} \Big|_{\chi_e = \chi_{e0}} = \frac{\dot{\chi}_{\max}}{\sin\chi_{e0}} > 0 \tag{28}$$

from which we can see that (25) and (27) determine a lower bound for $F(\chi_e)$. This lower bound is

$$\begin{aligned} F_{\min}(\chi_e) &= V_g (-\mathcal{A}_1 \sin\chi_d + \mathcal{A}_2 \cos\chi_d) + \dot{\chi}_{\max} \sin\chi_{e0} \\ &\ge V_g (-|\mathcal{A}_1| - |\mathcal{A}_2|) + \dot{\chi}_{\max} \sin\chi_{e0} \\ &\ge \frac{\sqrt{51} - 7}{10} \dot{\chi}_{\max} > 0 \end{aligned} \tag{29}$$

By letting $0 < k_1 < \frac{\sqrt{51}-7}{10} \dot{\chi}_{\max}$, we get that $F(\chi_e) \ge k_1$ and further $\dot{\chi}_d \ge -\dot{\chi}_{\max} + k_1 \sin\chi_e$.

CASE 2. $\chi_e \in (-\pi, 0)$

In this case, we have $\sin\chi_e \in (-1, 0)$. By considering another function

$$F(\chi_e) = \frac{1}{\sin\chi_e} (\dot{\chi}_d - \dot{\chi}_{\max}) \tag{30}$$

the conclusion $\dot{\chi}_d \le \dot{\chi}_{\max} + k_1 \sin\chi_e$ can be drawn similarly as before by taking the same k_1.

CASE 3. $\chi_e = 0$ or π

In this case, it can be easily seen that (22) holds by choosing an arbitrary positive k_1 by noticing $\sin\chi_e = 0$. ∎

It needs to be noted that (21) is a conservative condition for (22), which implies that the path following might still be achieved even $\mathcal{A}_1$ and $\mathcal{A}_2$ violate this condition. This lemma shows us that under condition (21), the maximum desired course rate of the combined vector field (13) is less than the course rate constraint $\dot{\chi}_{\max}$ regardless of the course error χ_e. This guarantees the feasibility of this vector field under the input constraint.

Condition (21) can be used to choose an appropriate parameter κ for the path following. As an illustrative example, consider a straight line given by $f(x, y) = ax + by + c = 0$. In this situation, $\mathcal{A}_1 = -a\kappa \mathrm{sech}(\kappa f)$ and $\mathcal{A}_2 = -b\kappa \mathrm{sech}(\kappa f)$. Then making use of (21), κ can be chosen to satisfy $\kappa \le 7\dot{\chi}_{\max} \Big/ \Big(10V_g(|a| + |b|)\Big)$.

Lemma 2: Given controller (19) and condition (21), there exists a positive constant k_2 such that

$$\begin{cases} \dot{\chi}_e \le -k_2 \sin\chi_e, & \text{if } \chi_e \in (0, \pi] \\ \dot{\chi}_e \ge -k_2 \sin\chi_e, & \text{if } \chi_e \in (-\pi, 0] \end{cases} \tag{31}$$

Proof: From (19) we have

$$\dot{\chi}_e = \dot{\chi} - \dot{\chi}_d = \begin{cases} -k_\chi \chi_e, & \text{if } \left|-k_\chi \chi_e + \dot{\chi}_d\right| \le \dot{\chi}_{\max} \\ \dot{\chi}_{\max} - \dot{\chi}_d, & \text{if } -k_\chi \chi_e + \dot{\chi}_d > \dot{\chi}_{\max} \\ -\dot{\chi}_{\max} - \dot{\chi}_d, & \text{if } -k_\chi \chi_e + \dot{\chi}_d < -\dot{\chi}_{\max} \end{cases} \tag{32}$$

Let us discuss this from two cases.

CASE 1. $\chi_e \in (0, \pi]$

In this case, $\sin\chi_e \ge 0$. If $\left|-k_\chi \chi_e + \dot{\chi}_d\right| \le \dot{\chi}_{\max}$, then we have $\dot{\chi}_e = -k_\chi \chi_e \le -k_2 \sin\chi_e$ by choosing a k_2 such that $0 < k_2 \le k_\chi$. If $-k_\chi \chi_e + \dot{\chi}_d > \dot{\chi}_{\max}$, then $\dot{\chi}_e = \dot{\chi}_{\max} - \dot{\chi}_d < -k_\chi \chi_e$. The same k_2 can be chosen to make $\dot{\chi}_e \le -k_2 \sin\chi_e$. Finally if $-k_\chi \chi_e + \dot{\chi}_d < -\dot{\chi}_{\max}$, we can see from **Lemma 1** that $\dot{\chi}_e = -\dot{\chi}_{\max} - \dot{\chi}_d \le -k_1 \sin\chi_e$. Then a k_2 satisfying $0 < k_2 \le k_1$ can be chosen to make $\dot{\chi}_e \le -k_2 \sin\chi_e$. In conclusion we obtain that there exists a positive constant k_2 subject to $k_2 \le \min\{k_\chi, k_1\}$ that can ensure $\dot{\chi}_e \le -k_2 \sin\chi_e$.

CASE 2. $\chi_e \in (-\pi, 0]$

In this case, following similar analysis as in the first case, we conclude that the same positive constant $0 < k_2 \le \min\{k_\chi, k_1\}$ can be chosen to make that $\dot{\chi}_e \ge -k_2 \sin\chi_e$. ∎

We can see from (31) that $\chi_e \dot{\chi}_e \le -k_2 \chi_e \sin\chi_e \le 0$. This implies that regardless of the original value, the absolute value of χ_e decreases with time under controller (19). This further means that UAV course will gradually reach the desired course determined by the guidance vector field.

Lemma 3: Assume that $\sqrt{f_x^2 + f_y^2} \le M$ with $M > 0$. Given controller (19) and condition (21), the directional distance r is bounded, i.e., there exists a positive constant K such that $|r| \le K$.

Proof: It can be seen from **Lemma 2** that $\dot{\chi}_e / \sin\chi_e \le -k_2$. Denoting the initial course error as χ_{e0}, and noticing that

$$\frac{\dot{\chi}_e}{\sin\chi_e} = \frac{\mathrm{d}\left[\log\left|\tan\left(\frac{\chi_e}{2}\right)\right|\right]}{\mathrm{d}t} \tag{33}$$

we obtain

$$\left|\tan\left(\frac{\chi_e}{2}\right)\right| \le \left|\tan\left(\frac{\chi_{e0}}{2}\right)\right| \mathrm{e}^{-k_2 t} \tag{34}$$

Evaluating the time derivative of r, we get

$$\dot{r} = f_x \dot{x} + f_y \dot{y} = V_g \sqrt{f_x^2 + f_y^2} \sin(\chi_e + \chi_r) \tag{35}$$

where $\chi_p = \arctan2(-f_x, f_y)$, and $\chi_r = \chi_d - \chi_p$. It needs to be noted that χ_p is the tangential direction of the curve corresponding to the current UAV location. Simplification of $\cos(\chi_d - \chi_p)$ yields that $\cos\chi_r = \mathrm{sech}(\kappa f) \ge 0$, from which we see that $\chi_r \in (-\pi/2, \pi/2)$. Similarly we have $\sin\chi_r = -\tanh(\kappa f)$, from which we further find that $\chi_r \in (-\pi/2, 0]$ when $r \ge 0$ and $\chi_r \in [0, \pi/2)$ when $r \le 0$. In the following we only consider the case when $r \ge 0$. The situation of the opposite case is similar to this.

When $\chi_e \in (0, \pi]$, according to **Lemma 2**, we have $\dot{\chi}_e \le -k_2 \sin\chi_e \le 0$, which indicates that $0 \le \chi_e \le \chi_{e0} \le \pi$. This further leads to $-\pi/2 \le \chi_e + \chi_r \le \chi_{e0} + \chi_r \le \pi$. If $-\pi/2 \le \chi_{e0} + \chi_r \le 0$, then we find that $\dot{r} \le 0$ from (35). This results in $r \le r_0$. If $0 < \chi_{e0} + \chi_r \le \pi$, then $\dot{r} \ge 0$, which implies that r will increase. Since the course error χ_e and χ_r as well are decreasing, the increasing of r stops when $\chi_e + \chi_r$ becomes zero, i.e., when $\chi_e = -\chi_r > 0$. According to (34), an upper bound of the time period for χ_e changing from χ_{e0} to $-\chi_{r0}$ can be given by

$$t_1 = \log\left|\frac{\tan\left(\frac{\chi_{e0}}{2}\right)}{\tan\left(\frac{-\chi_{r0}}{2}\right)}\right| \tag{36}$$

Instead of the unknown eventual χ_r, we use the conservative initial counterpart χ_{r0}. Then an upper bound for r can be computed as $r \le r_1 = r_0 + M(V_a + W)t_1$. Here $\dot{r} \le V_g M \le (V_a + W)M$ is used.

When $\chi_e \in (-\pi, 0]$, (31) gives us that $\dot{\chi}_e \ge -k_2 \sin\chi_e \ge 0$. This further gives $-\pi \le \chi_{e0} \le \chi_e \le 0$. Recalling that $\chi_r \in (-\pi/2, 0]$, we have $-3\pi/2 \le \chi_{e0} + \chi_r \le \chi_e + \chi_r \le 0$. If $-\pi \le \chi_{e0} + \chi_r \le 0$, then from (35) we can see that $\dot{r} \le 0$, which means $r \le r_0$. If $-3\pi/2 \le \chi_{e0} + \chi_r \le -\pi$, then $\dot{r} \ge 0$. Similarly r increases until $\chi_e + \chi_r = -\pi$, i.e., $\chi_e = -\pi - \chi_r < 0$. The time period of r's increasing is not more than

$$t_2 = \log\left|\frac{\tan\left(\frac{\chi_{e0}}{2}\right)}{\tan\left(\frac{-\pi - \chi_{r0}}{2}\right)}\right| \tag{37}$$

In this case the upper bound for r is $r_2 = r_0 + M(V_a + W)t_2$.

It can be seen from the above discussion that $0 \le r \le K_1 = \max\{r_1, r_2\}$. Following similar analysis for the case when $r \le 0$, we find that there exists a positive constant such that $|r| \le K_2$. Then the positive constant K which is used to bound r can be chosen as $K = \max\{K_1, K_2\}$. ∎

Now the proof of **Theorem 1** can be given as follows.

Proof of Theorem 1: Let us consider the Lyapunov function candidate

$$V_2 = \frac{1}{2}r^2 + \frac{\lambda}{2}\chi_e^2 \tag{38}$$

where $\lambda > 0$ is an adjustable scaling factor. Its time derivative is given by

$$\dot{V}_2 = r\dot{r} + \lambda\chi_e\dot{\chi}_e \leq fV_g\sqrt{f_x^2 + f_y^2}\sin(\chi_e + \chi_r) - \lambda k_2\chi_e\sin\chi_e \tag{39}$$

When $\chi_e = \pi$, it can be seen from (32) that $\dot{\chi_e} \neq 0$, which implies that χ_e will fall into $(-\pi, \pi)$. Thus we just consider the situation of $\chi_e \in (-\pi, \pi)$ as below.

CASE 1. $|\chi_e| \in (\pi/2, \pi)$

In this case we can see that $\chi_e \sin\chi_e \geq \pi/2\,|\sin\chi_{e0}|$. Thus if we take $\lambda \geq 2KM(V_a + W)/(\pi k_2\,|\sin\chi_{e0}|)$, then we have

$$\dot{V}_2 \leq KM(V_a + W) - \frac{\pi\lambda k_2}{2}\,|\sin\chi_{e0}| \leq 0 \tag{40}$$

CASE 2. $\chi_e \in [-\pi/2, \pi/2]$

In this case it can be easily found that $\chi_e \sin\chi_e \geq \sin^2\chi_e \geq \sin^2(\chi_e/2) \geq 0$. This yields

$$\begin{aligned}
\dot{V}_2 &\leq fV_g\sqrt{f_x^2 + f_y^2}\,[\sin\chi_e\cos\chi_r + \cos\chi_e\sin\chi_r] - \lambda k_2\sin^2\left(\frac{\chi_e}{2}\right)\\
&= fV_g\sqrt{f_x^2 + f_y^2}\left[2\sin\left(\frac{\chi_e}{2}\right)\cos\left(\frac{\chi_e}{2}\right)\cos\chi_r\right.\\
&\quad\left.+\left(1 - 2\sin^2\left(\frac{\chi_e}{2}\right)\right)\sin\chi_r\right] - \lambda k_2\sin^2\left(\frac{\chi_e}{2}\right)\\
&= fV_g\sqrt{f_x^2 + f_y^2}\sin\chi_r + 2fV_g\sqrt{f_x^2 + f_y^2}\sin\left(\frac{\chi_e}{2}\right)\cos\left(\chi_r + \frac{\chi_e}{2}\right)\\
&\quad-\lambda k_2\sin^2\left(\frac{\chi_e}{2}\right)\\
&\leq -V_g|f|\sqrt{f_x^2 + f_y^2}\,\tanh(\kappa|f|) + 2V_g|f|\sqrt{f_x^2 + f_y^2}\left|\sin\left(\frac{\chi_e}{2}\right)\right|\\
&\quad-\lambda k_2\left|\sin\left(\frac{\chi_e}{2}\right)\right|^2\\
&\leq -\sqrt{f_x^2 + f_y^2}\left[V_g\rho\,|f|^2 - 2V_g|f|\left|\sin\left(\frac{\chi_e}{2}\right)\right| + \frac{\lambda k_2}{\sqrt{f_x^2 + f_y^2}}\left|\sin\left(\frac{\chi_e}{2}\right)\right|^2\right]\\
&\leq -\sqrt{f_x^2 + f_y^2}\left[(V_a - W)\rho\,|f|^2 - 2(V_a + W)|f|\left|\sin\left(\frac{\chi_e}{2}\right)\right|\right.\\
&\quad\left.+\frac{\lambda k_2}{\sqrt{f_x^2 + f_y^2}}\left|\sin\left(\frac{\chi_e}{2}\right)\right|^2\right]
\end{aligned} \tag{41}$$

Here the fact that when $0 \leq x \leq K$ and $0 < \rho \leq \kappa\,\mathrm{sech}^2(\kappa K)/2$, the following expression satisfies

$$x\tanh(\kappa x) \geq \rho x^2 \tag{42}$$

is used. The proof of this fact is given in the Appendix. It can be seen from (41) that, if we take $\lambda \geq M(V_a + W)^2/(\rho k_2(V_a - W))$, then we have

$$\dot{V}_2 \leq -\sqrt{f_x^2 + f_y^2}\left[\sqrt{(V_a - W)\rho}\,|f| - \frac{\sqrt{\lambda k_2}}{\left(f_x^2 + f_y^2\right)^{1/4}}\left|\sin\left(\frac{\chi_e}{2}\right)\right|\right]^2 \leq 0 \tag{43}$$

For the Lyapunov function candidate V_2 given by (38), since $\dot{V}_2 \leq 0$ is guaranteed by (40) and (43), we conclude that $r \to 0$ and $\chi_e \to 0$ as $t \to +\infty$. $\chi_e \to 0$ means $\chi \to \chi_d$, which further leads to $\chi \to \chi_p$ by combining the conclusion $\chi_d \to \chi_p$. In fact we know from (14) that f decays to zero under the combined vector field (13). And $f \to 0$ further indicates that

$$\mathbf{v}_d = \frac{1}{\sqrt{f_x^2 + f_y^2}}\begin{pmatrix} f_y \\ -f_x \end{pmatrix} \tag{44}$$

This yields $\chi_d \to \chi_p$. This ends the proof of the theorem. ∎

IV. SIMULATION EXAMPLES

In this section simulation examples are given to verify the proposed path following approach. The sampling period of the controller is set to be 0.5 s. The constant airspeed for the UAV is $V_a = 20$ m/s. The constant wind velocity is assumed to be $\mathbf{W} = [6,8]$ m/s, which means that the wind speed accounts for 50 percent of the constant airspeed of the UAV. Course rate constraint is $\dot{\chi}_{\max} = 0.5$ rad/s. The feedback gain k_χ is chosen to be 1.

Assume that the UAV initially locates at (x_0, y_0). Then the initial directional distance between the UAV and the desired path can be computed by $r_0 = f(x_0, y_0)$. We consider the vector field parameter with the form $\kappa = \kappa_0/|r_0|$ to make κs dimensionless. Here κ_0 is set to be a positive constant, and is an alternative design parameter for κ. Moreover treating the initial distance $|r_0|$ as 1, we can calculate the relative distances at all discrete time instants.

Firstly a straight line path $y = 1.2x - 120$ is considered. We compare the path following results when κ_0 is taken to be four different constants, i.e., $\kappa_0 = 0.03$, 0.3, 3 and 10 (Fig. 2). From the comparison we can see that if κ_0 is too small, then the weighted conservative component of the combined vector field is not significant enough for rapid approach to the desired path. This results in very slow path following convergence. On the other hand if large κ_0 is chosen, several input saturations may happen in the beginning, which leads to trajectory oscillations around the desired path. And if κ_0 is too large, the desired course rate determined by the guidance vector field (15) may exceed the maximum course rate constraint of the UAV in a long time. This further results in extremely slow path following convergence with numbers of repeated trajectory oscillations. From the evaluation of the relative distances shown in Fig. 2(a), we can see that for different κ_0's which are smaller than a certain value, the larger κ_0 is, the smaller the relative distance at the same time instant is (i.e., the closer the UAV to the desired path is), and in addition the faster the path following convergence is.

We then consider the path following of a class of 2D sine curves $y = 500\sin((x - 800)/p) + 300$, where p is a designing parameter. Path following of two sine curves with $p = 100$ and $p = 170$ respectively is compared in this simulation. To obtain small following errors, and also to see the initial oscillations clearly, we intentionally choose a large vector field parameter. Specifically, we let $\kappa_0 = 30$. The results are given in Figs. 3-4. Figure 3 gives the relative distance comparison. It can be seen from Fig. 3 that unlike the case with large p, there exists some obvious spikes for the case with $p = 100$. These spikes indicates large path following errors, and their emergence coincides with the

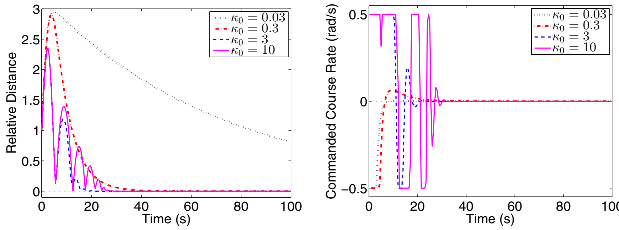

(a) (b)

Fig. 2. Path following of a straight line: (a) Relative distance from UAV to the straight line versus time; (b) Commanded course rate versus time.

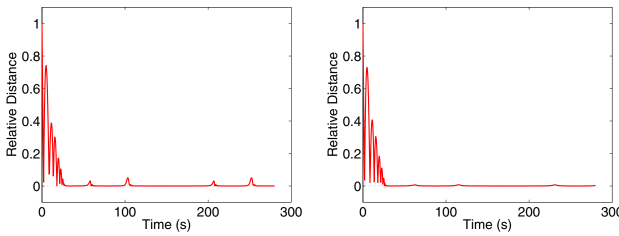

(a) (b)

Fig. 3. Relative distance from UAV to the sine curve versus time: (a) $p = 100$; (b) $p = 170$.

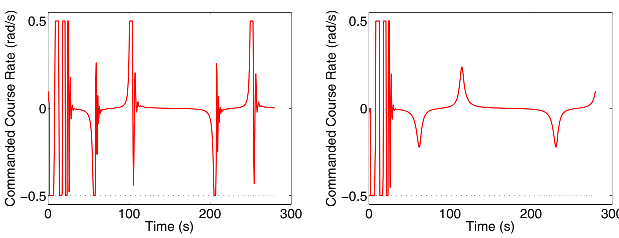

(a) (b)

Fig. 4. Commanded course rate comparison: (a) $p = 100$; (b) $p = 170$.

input saturations (See Fig. 3(a) and Fig. 4(a)). When $p = 170$, since no input saturation is involved after 60 s (Fig. 4(b)), no obvious distance spikes can be observed in Fig. 3(b), which implies better path following performance than the case when $p = 100$.

V. CONCLUSIONS

In this paper we have investigated the planar curved path following problem through the vector field approach. A combined vector field which combines a conservative vector field and a solenoidal vector field is proposed, based on which a saturated course rate controller is designed. The Lyapunov stability discussion is given in detail, which demonstrates the convergence of the vector field based controller under a path condition. Two simulation examples show us the effectiveness of the combined vector field based path following approach.

APPENDIX

A. *Proof of* (42)

Denote $f(x) = x\tanh(\kappa x) \geq 0$ and $g(x) = \rho x^2 \geq 0$. Then we can get that

$$\frac{\mathrm{d}f(x)}{\mathrm{d}x} = \tanh(\kappa x) + \kappa x\,\mathrm{sech}^2(\kappa x) \geq \kappa x\,\mathrm{sech}^2(\kappa x)$$

$$\geq \kappa x\,\mathrm{sech}^2(\kappa K) \geq 2\rho x = \frac{\mathrm{d}g(x)}{\mathrm{d}x} \tag{45}$$

In combination with the fact $f(0) = g(0) = 0$, we can see that (42) holds when $0 \leq x \leq K$ and $0 < \rho \leq \kappa\,\mathrm{sech}^2(\kappa K)/2$.

REFERENCES

[1] R. Austin, Unmanned Aircraft Systems: UAVS Design, Development and Deployment. Chichester, UK: John Wiley & Sons Ltd, 2010.

[2] D.R. Nelson, D.B. Barber, T.W. McLain, and R.W. Beard, Vector field path following for miniature air vehicles, IEEE Trans. Robot., vol. 23, pp. 519–529, Jun. 2007.

[3] I. Kaminer, A. Pascoal, E. Xargay, N. Hovakimyan, C. Cao, and V. Dobrokhodov, Path following for small unmanned aerial vehicles using L_1 adaptive augmentation of commercial autopilots. J. Guid. Contr. Dynam., vol. 33, pp. 550–564, Mar.-Apr. 2010.

[4] P.B. Sujit, S. Saripalli, and J.B. Sousa, Unmanned aerial vehicle path following: A survey and analysis of algorithms for fixed-wing unmanned aerial vehicles, IEEE Contr. Syst. Mag., vol. 34, pp. 42–59, Feb. 2014.

[5] E.W. Frew, D.A. Lawrence, and S. Morris, Coordinated standoff tracking of moving targets using Lyapunov guidance vector fields, J. Guid. Contr. Dynam., vol. 31, pp. 290–306, Mar.-Apr. 2008.

[6] D.A. Lawrence, E.W. Frew, and W.J. Pisano, Lyapunov vector fields for autonomous unmanned aircraft flight control, J. Guid. Contr. Dynam., vol. 31, pp. 1220–1229, Sep.-Oct. 2008.

[7] T.H. Summer, M.R. Akella, and M.J. Mears, Coordinated standoff tracking of moving targets: Control laws and information architectures, J. Guid. Contr. Dynam., vol. 32, pp. 56–69, Jan.-Feb. 2009.

[8] S. Zhu, D. Wang, and Q. Chen, Standoff tracking control of moving target in unknown wind, in Proceedings of Joint 48th IEEE Conference on Decision and Control and 28th Chinese Control Conference, Shanghai, China, 2009, pp. 776–781.

[9] S. Zhu, D. Wang, and C. Low, Ground target tracking using UAV with input constraints, J. Intell. Robot. Syst., vol. 69, pp. 417–429, Jan. 2013.

[10] H. Chen, K. Chang, and C.S. Agate, UAV path planning with tangent-plus-Lyapunov vector field guidance and obstacle avoidance, IEEE Trans. Aero. Electron. Syst., vol. 49, pp. 840–856, Apr. 2013.

[11] D.J. Bennet, and C.R. McInnes, Verifiable control of a swarm of unmanned aerial vehicles, Proc. IME G - J. Aero. Eng., vol. 223, pp. 939–953, Jul. 2009.

[12] S. Lim, Y. Kim, D. Lee, and H. Bang, Standoff target tracking using a vector field for multiple unmanned aircrafts, J. Intell. Robot. Syst., vol. 69, pp. 347–360, Jan. 2013.

[13] H. Oh, S. Kim, H.S. Shin, A. Tsourdos, and B.A. White, Coordinated standoff tracking of groups of moving targets using multiple UAVs, in Proceedings of the 2013 21st Mediterranean Conference on Control & Automation (MED), Crete, Greece, 2013, pp. 969–977.

[14] R.W. Beard, J. Ferrin, and J. Humpherys, Fixed wing UAV path following in wind with input constraints, IEEE Trans. Contr. Syst. Tech., vol. 22, pp. 2103–2117, Nov. 2014.

[15] S. Griffiths, Vector field approach for curved path following for miniature aerial vehicles, in Proceedings of AIAA Guidance, Navigation, and Control Conference and Exhibit, Keystone, CO, USA, 2006, AIAA 2006–6467.

[16] K.D. Young, V.I. Utkin, and Ü. Özgüner, A control engineer's guide to sliding mode control, IEEE Trans. Contr. Syst. Tech., vol. 7, pp. 328–342, May 1999.

[17] W. Ren, and R.W. Beard, Trajectory tracking for unmanned air vehicles with velocity and heading rate constraints, IEEE Trans. Contr. Syst. Tech., vol. 12, pp. 706–716, Sep. 2004.

[18] E.-K. Poh, J.-L. Wang, and K.-V. Ling, Near optimal tracking solution for input constrained UAV using MPC, in Proceedings of AIAA Guidance, Navigation, and Control Conference and Exhibit, Toronto, Ontario, Canada, 2010, AIAA 2010-7550.